LA-UR--83-3074

DE84 001724

CONF-8310104--2

Los Alamos National Laboratory is operated by the University of California for the United States Department of Energy under contract W-7405-ENG-36.

TITLE: PROMPT FISSION NEUTRON SPECTRA AND AVERAGE PROMPT NEUTRON MULTIPLICITIES

AUTHOR(S): David G. Madland, T-2

J. Rayford Nix, T-9

SUBMITTED TO: The Specialists' Meeting on "Yields and Decay Data Fission Product Nuclides," October 24-27, 1983, Brookhaven National Laboratory, sponsored by the OECD/NEA Nuclear Data Committee.

DISCLAIMER

Los Alamos National Laboratory
Los Alamos, New Mexico 87545

PROMPT FISSION NEUTRON SPECTRA AND AVERAGE PROMPT NEUTRON MULTIPLICITIES

David G. Madland and J. Rayford Nix

Theoretical Division, Los Alamos National Laboratory
Los Alamos, New Mexico 87545, U.S.A

ABSTRACT

We present a new method for calculating the prompt fission neutron spectrum N(E) and average prompt neutron multiplicity $\bar{\nu}_p$ as functions of the fissioning nucleus and its excitation energy. The method is based on standard nuclear evaporation theory and takes into account (1) the motion of the fission fragments, (2) the distribution of fission-fragment residual nuclear temperature, (3) the energy dependence of the cross section σ_c for the inverse process of compound-nucleus formation, and (4) the possibility of multiple-chance fission. We use a triangular distribution in residual nuclear temperature based on the Fermi-gas model. This leads to closed expressions for N(E) and $\bar{\nu}_p$ when σ_c is assumed constant and readily computed quadratures when the energy dependence of σ_c is determined from an optical model. Neutron spectra and average multiplicities calculated with an energy-dependent cross section agree well with experimental data for the neutron-induced fission of ^{235}U and the spontaneous fission of ^{252}Cf. For the latter case, there are some significant inconsistencies between the experimental spectra that need to be resolved.

I. INTRODUCTION

Having been concerned thus far in this meeting with properties of the delayed neutrons emitted from fission fragments, it is time now to shift our attention to the prompt neutrons. Both the prompt fission neutron spectrum N(E) and average prompt neutron multiplicity $\bar{\nu}_p$ are required in the analysis of many types of fission measurements and in the design of nuclear reactors as well as in in many other applications. For these purposes, N(E) is usually represented by a Maxwellian or Watt spectrum with parameters determined from adjustments to experimental data, and $\bar{\nu}_p$ is also usually obtained experimentally [1]. Such approaches cannot be used to predict N(E) and $\bar{\nu}_p$ for fissioning nuclei or excitation energies that have not been studied

experimentally. Also, because they neglect several important physical effects, these approaches must fail beyond certain levels of precision.

The importance of a more fundamental calculation of the prompt fission neutron spectrum N(E) has been recognized recently, and several calculations based on conventional nulcear theory have been performed. Browne and Dietrich [2] and Batenkov et al. [3] have used Hauser-Feshbach theory to calculate N(E) for the spontaneous fission of ^{252}Cf. While removing the deficiencies inherent in the Maxwellian and Watt spectra, these approaches are sufficiently complicated that they are difficult to apply to a variety of fissioning nuclei and excitation energies. In another study for the spontaneous fission of ^{252}Cf, Märten et al. [4] used a complex cascade evaporation model to calculate N(E). A similar evaporation model has been used by Hu and Wang [5] to calculate N(E) and $\bar{\nu}_p$ for neutron-induced fission of ^{235}U, ^{238}U, and ^{239}Pu as functions of incident neutron energy.

With the goal of incorporating the relevant physical effects yet retaining sufficient simplicity to facilitate its practical application, we have also developed a new method for calculating the prompt fission neutron spectrum N(E) and average prompt neutron multiplicity $\bar{\nu}_p$ [6,7]. As illustrated in Sec. II, our method predicts N(E) and $\bar{\nu}_p$ as functions of the fissioning nucleus and its excitation energy, taking into account multiple-chance fission when it becomes energetically possible. Some comparisons with experimental data are made in Sec. III for the neutron-induced fission of ^{235}U and in Sec. IV for the spontaneous fission of ^{252}Cf. Because of the importance of the latter reaction as a standard, we perform least-squares adjustments of Maxwellian spectra and our present spectra to some recent experimental spectra for the spontaneous fission of ^{252}Cf. This uncovers some significant inconsistencies between the experimental spectra that need to be resolved. Our conclusions are presented in Sec. V.

II. SUMMARY OF NEW THEORY

We use standard nuclear evaporation theory to calculate the prompt fission neutron spectrum and the average prompt neutron multiplicity as functions of the fissioning nucleus and its excitation energy, for spontaneous as well as neutron-induced fission. We take into account the motion of the fission fragments from which the neutrons are emitted, the distribution of fission-fragment residual nuclear temperature resulting from fragment cooling as neutrons are emitted, the energy dependence of the cross section for the inverse process of compound-nucleus formation, and the possibility of multiple-chance fission. In this section we present a summary of our approach, but refer the reader to Refs. [6] and [7] for a complete description.

A. Calculation of Prompt Fission Neutron Spectra

We calculate the neutron energy spectrum in the center-of-mass system of a given fission fragment and then transform to the laboratory system, taking into account that the average velocity of the light fragment is higher than that of the heavy fragment. The center-of-mass neutron energy spectrum

corresponding to a fixed residual nuclear temperature T is given approximately by [8,9]

$$\phi(\varepsilon) = k(T)\sigma_c(\varepsilon)\ \varepsilon\ \exp(-\varepsilon/T) \quad , \tag{1}$$

where ε is the center-of-mass neutron energy, $\sigma_c(\varepsilon)$ is the cross section for the inverse process of compound-nucleus formation, and $k(T)$ is the temperature-dependent normalization constant given by

$$k(T) = \left[\int_0^\infty \sigma_c(\varepsilon)\ \varepsilon\ \exp(-\varepsilon/T)d\varepsilon\right]^{-1} \quad . \tag{2}$$

This spectrum, along with all other distributions in this paper unless otherwise noted, is normalized to unity when integrated from zero to infinity.

As stressed by Weisskopf [8], T is not the temperature of the evaporating compound nucleus at excitation energy E*, but is instead the temperature of the residual nucleus at an excitation energy $E^* - B_n$ that is diminished by the neutron separation energy B_n. The prompt fission neutron spectrum depends strongly on the distribution of fission-fragment excitation energy E* and only weakly on the distributions of fission-fragment mass and kinetic energy. Therefore, we take into account the former distribution, but use average values for the last two distributions unless high accuracy is required as in, for example, a fission neutron spectrum standard.

The initial distribution of total fission-fragment excitation energy is approximately Gaussian in shape, with a total average value that is given by

$$\langle E^* \rangle = \langle E_r \rangle + B_n + E_n - \langle E_f^{tot} \rangle \quad . \tag{3}$$

Here, $\langle E_r \rangle$ is the average energy release, B_n and E_n are the separation and kinetic energies of the neutron inducing fission, and $\langle E_f^{tot} \rangle$ is the total average fission-fragment kinetic energy. For spontaneous fission, both B_n and E_n in Eq. (3) are zero.

Starting with an initial distribution of fission-fragment excitation energy obtained from experimental distributions of fission-fragment kinetic energy and neutron number, Terrell [10] summed the residual distributions following the emission of successive neutrons to obtain the distribution of excitation energy that governs neutron emission. This distribution was then transformed into the distribution P(T) of fission-fragment residual nuclear temperature by use of the Fermi gas model, where the excitation energy E* is related to the nuclear temperature T and the nuclear level density parameter a by

$$E^* = aT^2 \quad .$$

The resulting temperature distribution is approximately triangular in shape, with a moderately broad high-temperature cutoff.

Terrell observed that if this diffuse cutoff is replaced by a sharp cutoff, so that P(T) is approximated by the triangular distribution

$$P(T) = \begin{cases} 2T/T_m^2 , & T \le T_m \\ 0 , & T > T_m , \end{cases} \tag{4}$$

then the maximum temperature T_m is related to the initial total average fission-fragment excitation energy $\langle E^* \rangle$ approximately by

$$T_m = (\langle E^* \rangle / a)^{1/2} . \tag{5}$$

Equations (1) and (4) form the basis of our calculation of the prompt fission neutron spectrum. We consider two cases in calculating the spectrum.

In the first case, the cross section for the inverse process of compound-nucleus formation is assumed constant, which leads to a closed-form expression for the spectrum. The integral of this spectrum over an arbitrary finite energy range is also of closed form, which has important practical significance. In the second case, the energy dependence of the cross section for the inverse process of compound-nucleus formation is explicitly taken into account by use of an optical model. This spectrum is obtained by numerical integration and is a more accurate spectrum than that of the first case.

1. Constant Compound Nucleus Cross Section

If the compound nucleus cross section has a constant value σ_c, the normalization integral k(T) has the value $1/(\sigma_c T^2)$. The neutron energy spectrum in the center-of-mass system of a fission fragment is then obtained by integrating Eq. (1) over the triangular temperature distribution given by Eq. (4). This yields

$$\Phi(\varepsilon) = \int_0^\infty \phi(\varepsilon) P(T) dT = \frac{2\varepsilon}{T_m^2} \int_0^{T_m} \frac{\exp(-\varepsilon/T)}{T} dT = \frac{2\varepsilon}{T_m^2} E_1(\varepsilon/T) , \tag{6}$$

where

$$E_1(x) = \int_x^\infty \frac{\exp(-u)}{u} du$$

is the exponential integral [11]. This result has been obtained previously by Kapoor et al [12].

Although $\Phi(\varepsilon)$ itself is given in terms of an exponential integral, the moments $\langle \varepsilon^n \rangle$ of this distribution can all be evaluated simply by interchang-

ing the order of integration, which leads to

$$\langle \varepsilon^n \rangle = \int_0^\infty \varepsilon^n \phi(\varepsilon) d\varepsilon = \frac{2(n+1)!}{n+2} T_m^n \quad . \tag{7}$$

In particular, the mean energy and mean-square energy are given by

$$\langle \varepsilon \rangle = \frac{4}{3} T_m \tag{8}$$

and

$$\langle \varepsilon^2 \rangle = 3T_m^2 \quad . \tag{9}$$

We transform the spectrum given by Eq. (6) from the center-of-mass system of a fission fragment to the laboratory system, under the assumption that the neutrons are emitted istropically from a fission fragment moving with average kinetic energy per nucleon E_f. This is accomplished by use of the general result [10,13]

$$N(E,E_f) = \frac{1}{4\sqrt{E_f}} \int_{(\sqrt{E}-\sqrt{E_f})^2}^{(\sqrt{E}+\sqrt{E_f})^2} \frac{\Phi(\varepsilon)}{\sqrt{\varepsilon}} d\varepsilon \quad , \tag{10}$$

where E is the laboratory neutron energy. Upon inserting Eq. (6) and interchanging the order of integration, we obtain for the laboratory prompt fission neutron energy spectrum of one of the fragments

$$N(E,E_f) = \frac{1}{3(E_f T_m)^{1/2}} [u_2^{3/2} E_1(u_2) - u_1^{3/2} E_1(u_1) + \gamma(\tfrac{3}{2},u_2) - \gamma(\tfrac{3}{2},u_1)] \quad , \tag{11}$$

where

$$u_1 = (\sqrt{E} - \sqrt{E_f})^2 / T_m \quad ,$$

$$u_2 = (\sqrt{E} + \sqrt{E_f})^2 / T_m \quad ,$$

and

$$\gamma(a,x) = \int_0^x u^{1} \exp(-u)du$$

is the incomplete gamma function [14]. This spectrum can be calculated readily on a modern computer, as both the exponential integral and the incomplete gamma function are usually standard library functions. For applied purposes we present in Ref. [6] a closed-form expression for the integral of Eq. (11) over an arbitrary energy interval.

From conservation of momentum it follows that the average kinetic energy per nucleon of the light fragment is given by

$$E_f^L = \frac{A_H}{A_L} \frac{\langle E_f^{tot} \rangle}{A} \quad , \tag{12}$$

where

$\langle E_f^{tot} \rangle$ = total average fission-fragment kinetic energy

A = mass number of the compound nucleus undergoing fission

A_L and A_H = average mass numbers of the light and heavy fragments, respectively.

Similarly, the average kinetic energy per nucleon of the heavy fragment is

$$E_f^H = \frac{A_L}{A_H} \frac{\langle E_f^{tot} \rangle}{A} \quad . \tag{13}$$

For the fission of actinide nuclei, the average number of neutrons emitted from a given fragment depends strongly on fragment mass in accordance with the familiar sawtooth curve [1,15]. However, in the vicinity of the average fragments, the average numbers of neutrons emitted from the light and heavy fragments are approximately equal [1,15]. Accordingly, we equate the prompt fission neutron spectrum to the average of the spectra calculated for the light and heavy fragments. The laboratory prompt fission neutron energy spectrum N(E) is therefore written as

$$N(E) = \frac{1}{2} [N(E,E_f^L) + N(E,E_f^H)]. \tag{14}$$

The mean and mean-square energies for this spectrum are given by

$$\langle E \rangle = \frac{1}{2} (E_f^L + E_f^H) + \frac{4}{3} T_m \tag{15}$$

and

$$\langle E^2 \rangle = \frac{1}{2}\left[(E_f^L)^2 + (E_f^H)^2\right] + \frac{20}{9}(E_f^L + E_f^H)T_m + 3T_m^2 \quad . \tag{16}$$

We now discuss some illustrative examples of the laboratory prompt fission neutron spectrum given in Eq. (14). In these examples, as well as in all others given in Sec. II, we use values of the constants as determined in Ref. [6].

The spectrum calculated from Eq. (14) is shown by the solid curve in Fig. 1 for the fission of ^{235}U induced by 0.53-MeV neutrons. This reaction is chosen because of the existence of recent experimental data on the prompt fission neutron spectrum [16]. The dashed curve in Fig. 1 shows the Watt spectrum that is obtained by approximating $\Phi(\varepsilon)$ by a center-of-mass Maxwellian spectrum and by using the same average kinetic energy per nucleon E_f, from the average of Eqs. (12) and (13), for both the light and heavy fragments. Transformation to the laboratory system by use of Eq. (10) yields

$$N(E) = \frac{\exp(-E_f/T_W)}{(\pi E_f T_W)^{1/2}} \sinh[2(E_f E)^{1/2}/T_W]\exp(-E/T_W) \quad , \tag{17}$$

where the effective Watt temperature T_W is given by

$$T_W = \frac{8}{9} T_m \quad .$$

By construction, the mean laboratory neutron energy for this spectrum is equal to that given by Eq. (15) for the exact spectrum.

The dot-dashed curve in Fig. 1 shows the laboratory Maxwellian spectrum

$$N(E) = \frac{2\sqrt{E}\,\exp(-E/T_M)}{\sqrt{\pi}\,T_M^{3/2}} \quad , \tag{18}$$

where the effective Maxwellian temperature

$$T_M = \frac{1}{3}(E_f^L + E_f^H) + \frac{8}{9} T_m$$

is determined by requiring that the mean laboratory neutron energy of this spectrum be equal to that given by Eq. (15) for the exact spectrum.

As can be seen more clearly in Fig. 2, where we plot the ratio of these two approximations to the exact spectrum, the Watt spectrum is accurate to within a few per cent for laboratory neutron energies between 0 and ~ 7 MeV. For higher energies, the Watt spectrum is smaller than the exact spectrum because the Watt temperature T_W is smaller than the maximum temperature T_m.

In practice, the Watt spectrum is usually increased at high energies to better reproduce experimental data there by increasing T_W and decreasing E_f to values that are somewhat unphysical.

The Maxwellian spectrum, which neglects the motion of the fission fragments from which the neutrons are emitted, is a less accurate approximation. The Maxwellian spectrum is larger than the exact spectrum for laboratory neutron energies between 0 and ~ 1 MeV, whereas it is smaller for energies between ~ 1 and 5 MeV. For higher energies it is larger than the exact spectrum because the Maxwellian temperature T_m, which must account for the motion of the fission fragments as well as the center-of-mass motion of the neutrons, is larger than the maximum temperature T_m. In practice, the Maxwellian spectrum is usually decreased at high energies to better reproduce experimental data there by decreasing T_m. To preserve the normalization, this simultaneously increases the spectrum somewhat at lower energies.

The spurious enhancement of the Maxwellian spectrum for energies below ~ 1 MeV ironically accounts for part of its popularity in practice. As shown in Sec. II.A, the energy dependence of the compound nucleus cross section σ_c increases the spectrum at low energies relative to that calculated for a constant cross section. For the wrong physical reason, the Maxwellian spectrum reproduces this increase at low neutron energies somewhat better than do other spectra calculated for a constant cross section.

Our approach provides definite predictions concerning the dependence of the spectrum on both the fissioning nucleus and the kinetic energy of the neutron inducing fission. Figure 3 shows how the spectrum increases at high energy and decreases at low energy as the charge of the fissioning nucleus increases, for thermal-neutron-induced fission. Figure 4 shows how the spectrum increases at high energy and decreases at low energy as the kinetic energy of the incident neutron increases, for the first-chance fission of ^{235}U. As discussed in Sec. II.B, the inclusion of multiple-chance fission processes at high incident neutron energy decreases the spectrum at high energy relative to that calculated for first-chance fission.

2. Energy-Dependent Compound-Nucleus Cross Section

When the energy dependence of the cross section $\sigma_c(\varepsilon)$ for the inverse process of compound nucleus formation is taken into accoun , the neutron energy spectrum in the center-of-mass system of a fission fragment is again obtained by integrating Eq. (1) over the triangular temperature distribution given by Eq. (4). We obtain

$$\Phi(\varepsilon,\sigma_c) = \frac{2\sigma_c(\varepsilon)\varepsilon}{T_m^2} \int_0^{T_m} k(T)T \exp(-\varepsilon/T)dT \quad . \tag{19}$$

The neutron energy spectrum $N(E,E_f)$ in the laboratory system for a fission fragment moving with average kinetic energy per nucleon E_f is obtained by inserting this result into Eq. (1). This yields

$$N(E,E_f,\sigma_c) = \frac{1}{2\sqrt{E_f}T_m^2} \int_{(\sqrt{E}-\sqrt{E_f})^2}^{(\sqrt{E}+\sqrt{E_f})^2} \sigma_c(\varepsilon)\sqrt{\varepsilon}d\varepsilon \int_0^{T_m} k(T)T \exp(-\varepsilon/T)dT \quad . \quad (20)$$

The center-of-mass neutron energy spectrum $\Phi(\varepsilon)$ is obtained by evaluating Eq. (19) for neutron emission from the light L and heavy H average fission fragments and averaging the results in accordance with the discussion of Eq. (14), namely,

$$\Phi(\varepsilon) = \frac{1}{2} [\Phi(\varepsilon,\sigma_c^L) + \Phi(\varepsilon,\sigma_c^H)] \quad . \quad (21)$$

The center-of-mass energy moments of this spectrum, $\langle\varepsilon^n\rangle$, are given by

$$\langle\varepsilon^n\rangle = \int_0^\infty \varepsilon^n\Phi(\varepsilon)d\varepsilon \quad . \quad (22)$$

The laboratory prompt fission neutron spectrum is obtained by evaluating Eq. (2) for light L and heavy H average fission fragments and averaging the results, namely

$$N(E) = \frac{1}{2} [N(E,E_f^L,\sigma_c^L) + N(E,E_f^H,\sigma_c^H)] \quad . \quad (23)$$

The laboratory energy moments $\langle E^n\rangle$ of this spectrum are given by

$$\langle E^n\rangle = \int_0^\infty E^n N(E)dE \quad . \quad (24)$$

Considering again the fission of ^{235}U induced by 0.53-MeV neutrons, we illustrate in Figs. 5 and 6 the laboratory prompt neutron energy spectrum calculated from Eq. (23) using energy-dependdent compound nucleus cross sections $\sigma_c(\varepsilon)$. Results are shown and compared to the constant cross section result for three choices of the optical model potential used to calculate $\sigma_c(\varepsilon)$. These potentials, which have been widely used in neutron scattering calculations, are due to Becchetti and Greenless [17], Wilmore and Hodgson [18], and Moldauer [19]. The potentials are utilized in Eq. (23) by calculating $\sigma_c(\varepsilon)$ for neutrons incident on the central fragment of both the light and heavy average fragment groups, in the present case ^{96}Sr and ^{140}Xe.

Inspection of the figures shows that the energy-dependent cross sections soften the laboratory spectrum above ~ 2 MeV and harden it below, relative to that calculated for a constant cross section. Also, a broad peak with a maximum enhancement of ~ 10% exists in the energy-dependent cross-section calculation relative to that for a constant cross section.

Thus, the effect of the energy-dependent cross sections is to change the shape of the calculated spectrum in such a way as to increase the probability for emission of low-energy neutrons and to decrease the probability for emission of high-energy neutrons. Correspondingly, the energy moments calculated with Eqs. (22) and (24) for energy-dependent cross sections, are smaller than those calculated with Eqs. (7) and (15-16), for constant cross sections. Finally, we note from Fig. 6 that detailed comparisons of experiment and theory in the high-energy tail of the spectrum require use of an optical potential based on relatively high-energy neutron scattering data in order to draw meaningful conclusions. Of the three potentials presented here, that of Becchetti and Greenless [17] best meets this requirement. We therefore use this potential in the remainder of the present work.

B. Calculation of Average Prompt Neutron Multiplicities

The excitation energy of fission fragments is dissipated primarily by prompt neutron emission and to a lesser extent by prompt gamma emission in cascade de-excitation processes. The average prompt neutron multiplicity $\bar{\nu}_p$ is the average total number of prompt neutrons emitted per fission from all contributing cascades. As in the case of the prompt fission neutron spectrum N(E), we calculate $\bar{\nu}_p$ as a function of both the fissioning nucleus and its excitation energy.

The total average fission-fragment excitation energy $\langle E^* \rangle$ is by energy conservation equal to the product of the average prompt neutron multiplicity $\bar{\nu}_p$ and the average energy removed per emitted neutron $\langle \eta \rangle$ plus the total average prompt gamma energy $\langle E_\gamma^{tot} \rangle$. Thus,

$$\langle E^* \rangle = \bar{\nu}_p \langle \eta \rangle + \langle E_\gamma^{tot} \rangle \quad . \tag{25}$$

The average energy removed per emitted neutron $\langle \eta \rangle$ has been studied by Terrell [20] and is represented reasonably well by the sum of the average fission-fragment neutron separation energy $\langle S_n \rangle$ and the average center-of-mass energy of the emitted neutrons $\langle \varepsilon \rangle$. Thus,

$$\langle \eta \rangle = \langle S_n \rangle + \langle \varepsilon \rangle \quad . \tag{26}$$

Combining Eqs. (25) and (26) and solving for $\bar{\nu}_p$ yields

$$\bar{\nu}_p = \frac{\langle E^* \rangle - \langle E_\gamma^{tot} \rangle}{\langle S_n \rangle + \langle \varepsilon \rangle} \quad . \tag{27}$$

In this equation the total average fission-fragment excitation energy $\langle E^* \rangle$ is already known as a function of the fissioning nucleus and its excitation energy and is given by Eq. (3). Similarly, the average center-of-mass energy of the emitted neutrons $\langle \varepsilon \rangle$ is identical to the mean energy of the center-of-mass prompt fission neutron spectrum $\Phi(\varepsilon)$ and is also known as

a function of both the fissioning nucleus and its excitation energy. For the case of a constant compound nucleus cross section, $\langle\varepsilon\rangle$ is given by Eq. (8), and for the case of an energy-dependent compound nucleus cross section, $\langle\varepsilon\rangle$ is given by Eq. (22).

We obtain the explicit expression for the average prompt neutron multiplicity $\bar{\nu}_p$ by inserting Eq. (3) into Eq. (27), which yields finally

$$\bar{\nu}_p = \frac{\langle E_r \rangle + B_n + E_n - \langle E_f^{tot} \rangle - \langle E_\gamma^{tot} \rangle}{\langle S_n \rangle + \langle \varepsilon \rangle} \quad . \tag{28}$$

This equation is valid for neutron-induced first-chance fission and spontaneous fission, in which case E_n and B_n are set equal to zero. In addition, the various terms of the average prompt neutron multiplicity for neutron-induced multiple-chance fission, to be discussed next, are constructed using this expression for first-chance fission. In Secs. III and IV we will compare experimental and calculated average prompt neutron multiplicities.

C. Multiple-Chance Fission

At incident neutron energies above ~ 6 MeV the excitation energy of the compound nucleus is sufficiently large that fission is possible following the emission of one or more neutrons. Consequently, Eqs. (14) or (23) for the prompt neutron spectrum N(E) and Eq. (28) for the average neutron multiplicity $\bar{\nu}_p$ must be solved for successive fissioning compound nuclei that occur in the competing multiple-chance fission reactions. The final expressions for N(E) and $\bar{\nu}_p$ are then obtained by combining the contributions from the individual competing reactions in proportion to their corresponding probabilities of occurrence. We present here the final equations for N(E) and $\bar{\nu}_p$ for the effects of and competition between multiple-chance fission processes up through third-chance fission and refer the reader to Ref. [6] for a complete derivation of these equations. We then illustrate these effects for the neutron-induced multiple-chance fission of ^{235}U.

The prompt fission neutron spectrum for neutron-induced, multiple-chance fission is obtained by construction, using the expression for the prompt fission neutron spectrum N(E) due to first-chance fission, the expression for the evaporation spectrum $\phi(E)$ due to neutron emission prior to fission, and the multiple-chance fission probabilities $P_{f_i}^A$. The total prompt fission neutron spectrum due to first-, second-, and third-chance fission events is given in the laboratory system by

$$N(E) = \{ P_{f_1}^A \bar{\nu}_{p_1} N_1(E) + P_{f_2}^A [\phi_1(E) + \bar{\nu}_{p_2} N_2(E)]$$

$$+ P_{f_3}^A [\phi_1(E) + \phi_2(E) + \bar{\nu}_{p_3} N_3(E)]\} / P_{f_1} \bar{\nu}_{p_1}$$

$$+ P^A_{f_2}(1 + \bar{\nu}_{p_2}) + P^A_{f_3}(2 + \bar{\nu}_{p_3})] \quad , \tag{29}$$

where E is the energy of the emitted neutron and A is the mass number of the fissioning compound nucleus. The first term of this equation is the first-chance fission component; the second and third terms are the second-chance fission component; and the fourth, fifth, and sixth terms are the third-chance fission component of the spectrum. The spectrum constructed in this way gives unit normalization when integrated from zero to infinity.

When Eq. (29) is evaluated as a function of incident neutron energy E_n, one obtains the prompt fission neutron spectrum matrix $N(E,E_n)$. This matrix is illustrated in Figs. 7 and 8 for the neutron-induced fission of ^{235}U up through third-chance fission. In Fig. 8 the ratio matrix $R(E,E_n) = N(E,E_n)/N(E,0)$ is illustrated to enhance fine details of the matrix. These figures clearly illustrate the dependence of the matrix upon the incident neutron energy E_n, particularly in the tail region corresponding to high secondary neutron energy E, where the matrix generally becomes harder with increasing E_n. As E_n increases beyond about 6 MeV, the tail region softens somewhat because part of the nuclear excitation energy is dissipated by the emission of a neutron prior to fission. This softening is observed again just beyond 13 MeV where the threshold for the emission of two neutrons prior to fission occurs.

We also obtain the average prompt neutron multiplicity for neutron-induced multiple-chance fission by construction, using the expression for the average prompt neutron multiplicity $\bar{\nu}_p$ due to first-chance fission and the multiple-chance fission probabilities $P^A_{f_i}$. The total average prompt neutron multiplicity due to first-, second-, and third-chance fission events is given by

$$\bar{\nu}_p = [P^A_{f_1}\nu_{p_1} + P^A_{f_2}(1 + \nu_{p_2}) + P^A_{f_3}(2 + \bar{\nu}_{p_3})]/(P^A_{f_1} + P^A_{f_2} + P^A_{f_3}) \quad , \tag{30}$$

We show a comparison of experimental and calculated average neutron multiplicities using this equation, as well as Eq. (28), in the next section.

III. SOME COMPARISONS WITH EXPERIMENT FOR THE NEUTRON-INDUCED FISSION OF ^{235}U

We first compare the spectra calculated for both a constant compound nucleus cross section σ_c and an energy-dependent cross section $\sigma_c(\varepsilon)$ with the experimental spectrum measured by Johansson and Holmqvist [11] for 0.53-MeV neutrons incident on ^{235}U. The comparisons are shown in Figs. 9 and 10. Figure 9 shows that both of the calculated spectra agree well with experiment although there is a clear preference for the energy-dependent cross-section calculation in the tail region of the spectrum above ~ 3 MeV. This preference can be seen more clearly in Fig. 10 where the ratios to the constant cross-section calculation are plotted. This figure shows conclusively that the energy dependent cross-section calculation is the physically preferred spectrum.

Second, we compare the calculated average prompt neutron multiplicity with experiment for the neutron-induced fission of ^{235}U for incident neutron energies ranging from thermal energy to 15 MeV. We compare the experimental data with two different calculations. The first calculation, shown by the dashed curve in Fig. 11, assumes that first-chance fission only is occurring, whereas the second and more realistic calculation, shown by the solid curve, includes the effects of first-, second-, and third-chance fission. In the first-chance fission region the two calculations are of course identical and agree well with experiment, although discrepancies as large as 3% occur near 5-MeV incident neutron energy. In the multiple-chance fission region beginning near 5.5 MeV, the agreement of both the first- and multiple-chance fission calculations with experiment is very good, of the order of 1%. The multiple-chance fission calculation introduces a smooth upward step at the second-chance fission threshold near 5.5 MeV and a very slight drop at the third-chance fission threshold near 12 MeV, relative to the smoother first-chance fission calculation. It appears therefore, for ^{235}U fission, that multiple-chance fission processes introduce only slight corrections to the calculation based on first-chance fission.

IV. PROMPT FISSION NEUTRON SPECTRUM AND AVERAGE PROMPT NEUTRON MULTIPLICITY FOR THE ^{252}Cf(sf) STANDARD REACTION

We now turn our attention to the prompt fission spectrum and average prompt nuetorn multiplicity for the spontaneous fission of ^{252}Cf. These are very important quantities as they are used as standards in many neutron physics measurements and in many areas in applied programs. Therefore, we use our energy-dependent cross-section calculation here. We have already reported our preliminary studies on ^{252}Cf at the 1982 Antwerp meeting in Ref. [16] and in this section we summarize our progress since that meeting.

As in Ref. [16], we take two important new steps to calculate N(E) and $\bar{\nu}_p$ for the ^{252}Cf(sf) reaction. The first of these is that we perform a complete integration for the average energy release in fission $\langle E_r \rangle$ without approximation instead of using our normal seven-point approximation. In so doing, we obtain mass values from the new 1981 Wapstra-Bos mass evaluation [17] when they exist and otherwise from the new macroscopic-microscopic mass formula of Möller and Nix [18]. The second step is that we perform a least-squares adjustment of our calculated spectrum to a well-measured experimental spectrum in order to determine the value of the nuclear level-density parameter a that enters our calculations of N(E) and $\bar{\nu}_p$ through Eq. (5). A least-squares adjustment is performed because we wish to obtain the most accurate representations of the physical spectrum and physical neutron multiplicity as is possible and we do so with respect to the nuclear level-density parameter because it is the least well-known parameter that enters our formalism. The average neutron multiplicity is not included in the least-squares adjustment because it depends only weakly on the nuclear level density, as shown by Eq. (28).

We perform the least-squares adjustments with respect to two recent measurements of the spectrum. The first of these is the measurement of Boldeman et al. [19], experiment no. 7, final data analysis [20], and the

second is the measurement of Poenitz and Tamura [21,22]. Our results are given in Figures 12-15 and in Tables I and II where they are compared with the two experimental measurements as well as with the results of least-square adjustments that we have performed with respect to a Maxwellian spectrum.

Considering first our results for the measurement of Boldeman et al. [19,20], shown in Figs. 12-13 and tabulated in Col. 1 of Tables I and II, we find that a Maxwellian spectrum with temperature T_m = 1.426 MeV gives a better value of χ^2_{min} than does our energy-dependent cross-section calculation with temperature T_m = 1.124 MeV. The values of χ^2_{min} are 1.175 and 3.529, respectively. Inspection of Fig. 13 indicates that the difference between the two χ^2_{min} values is due largely to contributions to χ^2 from the region 800 keV to about 1.1 MeV, wherein the Maxwellian spectrum is everywhere in better agreement with experiment than our calculated spectrum.

Considering second our results for the measurement of Poenitz and Tamura [21,22], shown in Figs. 14-15 and tabulated in Col. 2 of Tables I and II, we find that our energy-dependent cross-section calculation with temperature T_m = 1.094 MeV gives a better value of χ^2_{min} than does a Maxwellian spectrum with temperature T_m = 1.429 MeV. In this case, the values of χ^2_{min} are 0.552 and 1.201, respectively. Inspection of Fig. 15 indicates that the difference between the two χ^2_{min} values is not due to the preference of our calculated spectrum in a specific energy region, as is the case for the Maxwellian spectrum preference with the Boldeman et al. experiment, but is instead due to uniformly better agreement with the experiment over most of the experimental range.

Thus, we see that the two spectrum measurements are inconsistent with each other and that these inconsistencies, although slight, are significant because they lead to different conclusions as to what the shape and energy moments of the real physical spectrum are. Therefore, additional existing or new experimental measurements of this spectrum are required to determine exactly the prompt fission neutron spectrum for the ^{252}Cf(sf) standard reaction.

In closing, we note that our calculated values of $\bar{\nu}_p$ appearing in Table II are quite close to the experimental values of 3.757 ± 0.009, obtained from the measurements of Amiel [23] and Smith [24], and 3.773 ± 0.007, obtained by Spencer et al. [25].

V. CONCLUSIONS

We have formulated a new method for the calculation of the prompt fission neutron spectrum N(E) and the average prompt neutron multiplicity $\bar{\nu}_p$ that incorporates the known relevant physical effects and is sufficiently simple that it can be used in most applications. Our calculations agree well with experiment and where measurements do not exist, or are not possible, we are able to provide calculations of N(E) and $\bar{\nu}_p$ as a function of fissioning nucleus and excitation energy. In cases requiring maximum accuracy, our approach leads itself to least-squares adjustments of the spectrum with respect to the nuclear level-density parameter. In the case of the ^{252}Cf(sf) standard reaction, we have demonstrated small, but very significant, inconsistencies between two measurements of the spectrum that prevent

definitive conclusions on the physical shape of the spectrum and the values of the spectrum energy moments.

ACKNOWLEDGEMENTS

We are grateful to J. W. Boldeman and W. P. Poenitz for the use of their experimental data and for several stimulating discussions and communications concerning the prompt fission neutron spectrum for the spontaneous fission of ^{252}Cf.

REFERENCES

1. J. Terrell, Proc. Symposium on Physics and Chemistry of Fission, Salzburg, Austria, March 22-26, 1965, International Atomic Energy Agency, Vienna (1965), Vol. II, p. 3.

2. J. C. Browne and F. S. Dietrich, Phys. Rev. C 10, 2545 (1974).

3. O. I. Batenkov, M. V. Blinov, G. S. Boykov, V. A. Vitenko, and V. A. Rubchenya, Proc. Consultants' Meeting on the Californium-252 Fission-Neutron Spectrum, Smolenice, Czechoslovakia, March 28-April 1, 1983, International Atomic Energy Agency, Vienna (to be published).

4. H. Märlen, D. Neumann, and D. Seelinger, Proc. Consultants' Meeting on the Californium-252 Fission-Neutron Spectrum, Smolenice, Czechoslovakia, March 28-April 1, 1983, International Atomic Energy Agency, Vienna (to be published).

5. J. M. Hu and Z. S. Wang, Physica Energiae Fortis et Physica Nuclearis, 3, 772 (1979).

6. D. G. Madland and J. R. Nix, Nucl. Sci. Eng., 81, 213 (1982).

7. D. G. Madland and J. R. Nix, Proc. International Conference on Nuclear Data for Science and Technology, Antwerp, Belgium, September 6-10, 1982, Reidel, Dordrecht (1983) p. 473.

8. V. F. Weisskopf, Phys. Rev., 52, 295 (1937).

9. J. M. Blatt and V. F. Weisskopf, Theoretical Nuclear Physics, p. 365, John Wiley and Sons, Inc., New York (1952).

10. J. Terrell, Phys. Rev., 113, 527 (1959).

11. M. Abramowitz and I. A. Stegun, Eds., Handbook of Mathematical Functions, p. 227, National Bureau of Standards, Washington, D.C. (1964).

12. S. S. Kapoor, R. Ramanna, and P. N. Rama Rao, Phys Rev., 131, 283 (1963).

13. N. Feather, "Emission of Neutrons from Moving Fission Fragments," BM-148, Brittish Mission (1942).

14. M. Abramowitz and I. A. Stegun, Eds., Handbook of Mathematical Functions, p. 253, National Bureau of Standards, Washington, D.C. (1964).

15. J. Terrell, Phys. Rev., 127, 880 (1962).

16. P. I. Johansson and B. Holmqvist, Nucl. Sci. Eng., 62, 695 (1977).

17. F. D. Becchetti, Jr. and G. W. Greenless, Phys. Rev., 182, 1190 (1969).

18. D. Wilmore and P. E. Hodgson, Nucl. Phys., 55, 673 (1964).

19. F. Moldauer, Nucl. Phys., 47, 65 (1963).

20. J. Terrell, Phys. Rev., 108, 783 (1957).

21. A. H. Wapstra and K. Bos, private communication to the Nat. Nuclear Data Center, Brookhaven National Laboratory (March 1982).

22. P. Möller and J. R. Nix, At. Data Nucl. Data Tables 26, 165 (1981).

23. J. W. Boldeman, D. Culley, and R. J. Cawley, Trans. Am. Nucl Soc. 32, 733 (1979).

24. J. W. Boldeman, private communication (May 1983).

25. W. P. Poentiz and T. Mamura, Proc. International Conference for Science and Technology, Antwerp, Belgium, September 6-10, 1982, Reidel, Dordrecht (1983) p. 465.

26. W. P. Poenitz, private communication (April 1983).

27. S. Amiel, Proc. Second IAEA Symp. on Physics and Chemistry of Fission, Vienna, Austria, 1969 (International Atomic Energy Agency, Vienna, 1969), p. 569.

28. J. R. Smith, Proc. Symp. Nuclear Data Problems for Thermal Reactor Applications, Brookhaven National Laboratory, 1978, EPRI-NP-1093, Electric Power Research Institute (1979), p. 5-1.

29. R. R. Spencer, R. Gwin, and R. Ingle, Nucl. Sci. Eng. 80, 603 (1982).

FIGURE CAPTIONS

Fig.1. Prompt fission neutron spectrum in the laboratory system for the fission of ^{235}U induced by 0.53-MeV neutrons. The solid curve gives the present spectrum calculated from Eq. (14); the dashed curve gives the Watt

spectrum calculated from Eq. (17); and the dot-dashed curve gives the Maxwellian spectrum calculated from Eq. (18). The values of the three constants appearing in the present spectrum are E_f^L = 1.062 MeV, E_f^H = 0.499 MeV, and T_m = 1.019 MeV, whereas those in the Watt spectrum are E_f = 0.780 MeV and T_W = 0.905 MeV. The value of the single constant appearing in the Maxwellian spectrum is T_M = 1.426 MeV. The mean laboratory neutron energies of the three spectra are identical.

Fig. 2. Ratio of Watt spectrum and the Maxwellian spectrum to the present spectrum, corresponding to the curves shown in Fig. 1.

Fig. 3. Dependence of the prompt fission neutron spectrum on the fissioning nucleus, for thermal-neutron-induced fission. The values of the constants are E_f^L = 1.106 MeV, E_f^H = 0.457 MeV, and T_m = 0.989 MeV for ^{229}Th + n; E_f^L = 1.033 MeV, E_f^L = 0.527 MeV, and T_m = 1.124 MeV for ^{239}Pu + n; and E_f^L = 0.995 MeV, E_f^H = 0.575 MeV, and T_m = 1.304 MeV for ^{249}Cf + n.

Fig. 4. Dependence of the prompt fission neutron spectrum on the kinetic energy of the incident neutron for the fission of ^{235}U. The maximum temperature T_m is 1.006 MeV when the incident neutron energy is 0, 1.157 MeV when the incident neutron energy is 7 MeV, and 1.290 MeV when the incident neutron energy is 14 MeV. The values of the average kinetic energy per nucleon are for each case held fixed at E_f^L = 1.062 MeV and E_f^H = 0.499 MeV. For the last two cases, the spectra are calculated for the first-chance fission only.

Fig. 5. Prompt fission neutron spectra in the laboratory system for the fission of ^{235}U induced by 0.53-MeV neutrons. The short-dashed curve gives the spectrum for σ_c = constant calculated with Eq. (14) and is identical to the solid curve in Fig. 1. The remaining curves are calculated with Eq. (23), but differ by the choice of optical model potential used to calculate $\sigma_c(\varepsilon)$ for the average fragment of each mass peak. The solid curve gives the spectrum calculated using the potential of Becchetti and Greenless [12], the dot-dashed curve gives the spectrum calculated using the potential of Wilmore and Hodgson [18], and the long-dashed curve gives the spectrum calculated using the potential of Moldauer [19]. The values of the constants appearing in the spectra are E_f^L = 1.062 MeV, E_f^H = 0.499 MeV, and T_m = 1.019 MeV.

Fig. 6. Ratio of the spectra calculated using different optical model potentials to generate $\sigma_c(\varepsilon)$ to the spectrum calculated with σ_c = constant, corresponding to the curves shown in Fig. 5.

Fig. 7. Prompt fission neutron spectrum matrix $N(E,E_n)$ for the neutron-induced fission of ^{235}U as a function of incident neutron energy E_n and emitted neutron energy E.

Fig. 8. Prompt fission neutron spectrum ratio matrix $R(E,E_n) = N(E,E_n)/N(E,0)$ corresponding to the matrix shown in Fig. 7.

Fig. 9. Prompt fission neutron spectrum in the laboratory system for the fission of ^{235}U induced by 0.53-MeV neutrons. The dashed curve gives the spectrum calculated with Eq. (14) for a constant cross section, whereas the solid curve gives the spectrum calculated with Eq. (23) for energy-dependent cross sections obtained using the optical model potential of Becchetti and Greenlees [17]. The values of the constants appearing in the calculated spectra are $E_f^L = 1.062$ MeV, $E_f^H = 0.499$ MeV, and $T_m = 1.019$ MeV. The experimental data are those of Johansson and Holmqvist [16].

Fig. 10. Ratio of the spectrum calculated using energy-dependent cross sections and the experimental spectrum to the spectrum calculated using a constant cross section, corresponding to the curves shown in Fig. 9.

Fig. 11. Average prompt neutron multiplicity as a function of the incident energy for the neutron-induced fission of ^{235}U. The dashed curve gives the multiplicity calculated with Eq. (28) assuming first-chance fission, whereas the solid curve gives the multiplicity calculated with Eq. (30) assuming multiple-chance fission. In both cases, the optical model potential of Becchetti and Greenlees [17] is used to determine the center-of-mass energies used in the equations. The original sources for the experimental data are given in Ref. [6]. Note the suppressed zero of the verical scale.

Fig. 12. Prompt fission neutron spectrum in the laboratory system for the spontaneous fission of ^{252}Cf. The dashed curve gives the least-squares adjusted Maxwellian spectrum calculated with Eq. (18) and the solid curve gives the least-squares adjusted energy-dependent cross-section spectrum calculated with Eq. (23). The experimental data are those of Boldeman et al. [19] and Boldeman [20], experiment 7, final data.

Fig. 13. Ratio of the energy-dependent cross section spectrum and the experimental spectrum to the Maxwellian spectrum, corresponding to the curves shown in Fig. 12.

Fig. 14. Prompt fission neutron spectrum in the laboratory system to the spontaneous fission of ^{252}Cf. The dashed curve gives the least-squares adjusted Maxwellian spectrum calculated with Eq. (18) and the solid curve gives the least-squares adjusted energy-dependent cross-section spectrum calculated with Eq. (23). The experimental data are those of Poenitz and Tamura [21] and Poenitz [22].

Fig. 15. Ratio of the energy-dependent cross-section spectrum and the experimental spectrum to the Maxwellian spectrum, corresponding to the curves shown in Fig. 14.

TABLE I

Least-Squares Adjustments of Maxwellian Spectra for the Spontaneous Fission of ^{252}Cf

Quantity	Experimental Spectrum	
	Boldeman et al.[a]	Poenitz and Tamura[b]
Number of data points	95	51
Energy range of experiment (MeV)	0.801-14.239	0.225-9.800
Fraction of theoretical spectrum (1%)	77.13	95.39
T_M (MeV)	1.426	1.429
$\langle E \rangle$ (MeV)	2.139	2.144
$\langle E^2 \rangle$ (MeV^2)	7.626	7.658
χ^2_{min}	1.175	1.201

TABLE II

Least-Squares Adjustments of Present Energy-Dependent Cross-Section Spectra for the Spontaneous Fission of Cf

Quantity	Experimental Spectrum	
	Boldeman et al.[a]	Poenitz and Tamura[b]
Number of data points	95	51
Energy range of experiment (MeV)	0.801-14.239	0.225-9.800
Fraction of theoretical spectrum (1%)	78.80	95.99
a (1/MeV)	A/9.65	A/9.15
T_M (MeV)	1.124	1.094
$\langle E \rangle$ (MeV)	2.171	2.134
$\langle E^2 \rangle$ (MeV)	7.637	7.364
$\bar{\nu}_p$	3.789	3.810
χ^2_{min}	3.529	0.552

[a] Refs. [23] and [24]

[b] Refs. [29] and [26]

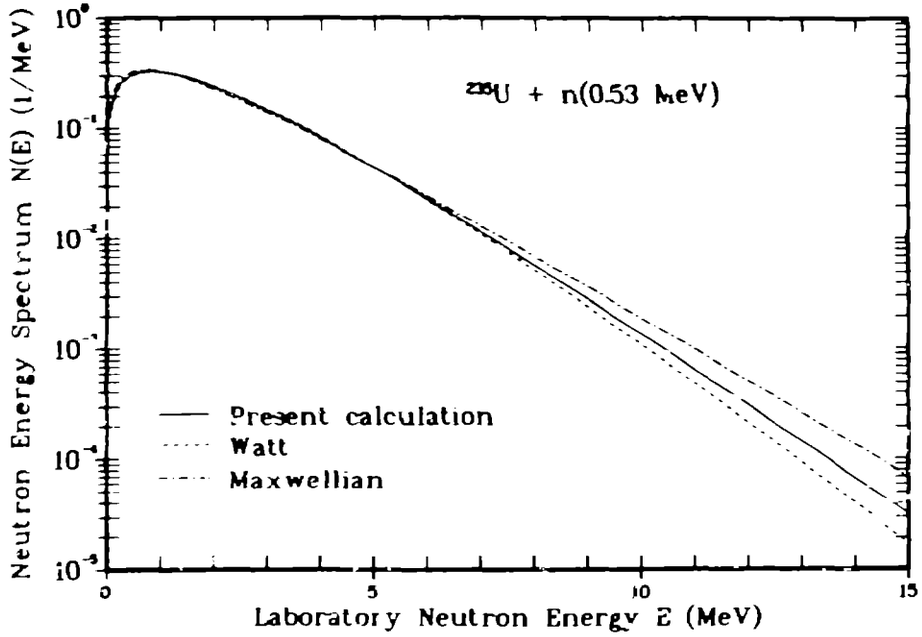
Neutron Energy Spectrum N(E) (1/MeV)
10^{0}
10^{-1}
10^{-2}
10^{-3}
10^{-4}
10^{-5}
^{238}U + n(0.53 MeV)
Present calculation
Watt
Maxwellian
0
5
10
15
Laboratory Neutron Energy E (MeV)

Fig. 1.

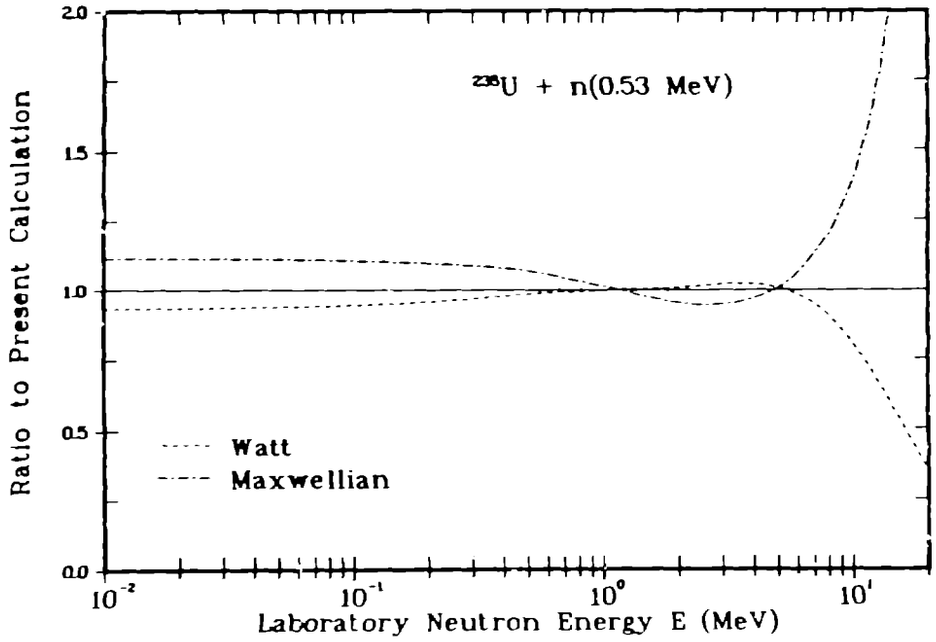
2.0
1.5
1.0
0.5
0.0
Ratio to Present Calculation
^{238}U + n(0.53 MeV)
Watt
Maxwellian
10^{-2}
10^{-1}
10^{0}
10^{1}
Laboratory Neutron Energy E (MeV)

Fig. 2.

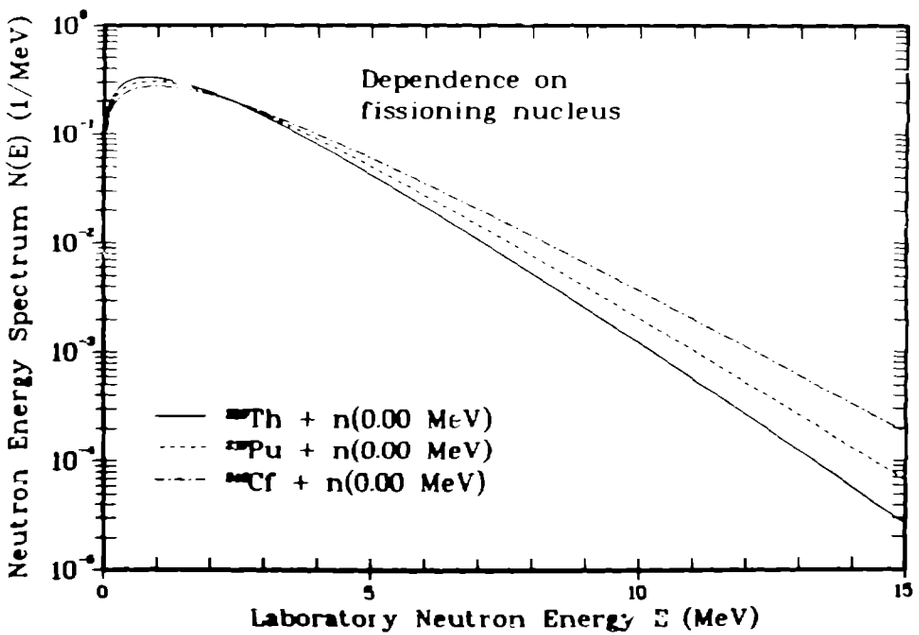
Dependence on
fissioning nucleus
Th + n(0.00 MeV)
Pu + n(0.00 MeV)
Cf + n(0.00 MeV)
Neutron Energy Spectrum N(E) (1/MeV)
Laboratory Neutron Energy E (MeV)
10^0
10^-1
10^-2
10^-3
10^-4
10^-5
0
5
10
15

Fig. 3.

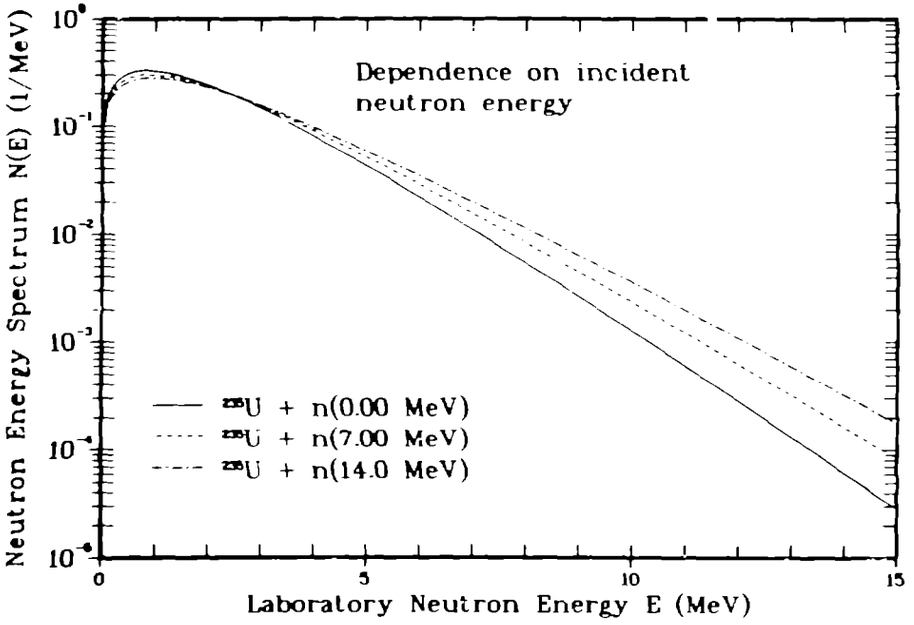
Dependence on incident
neutron energy
^{238}U + n(0.00 MeV)
^{238}U + n(7.00 MeV)
^{238}U + n(14.0 MeV)
Neutron Energy Spectrum N(E) (1/MeV)
Laboratory Neutron Energy E (MeV)
10^{0}
10^{-1}
10^{-2}
10^{-3}
10^{-4}
10^{-5}
0
5
10
15

Fig. 4.

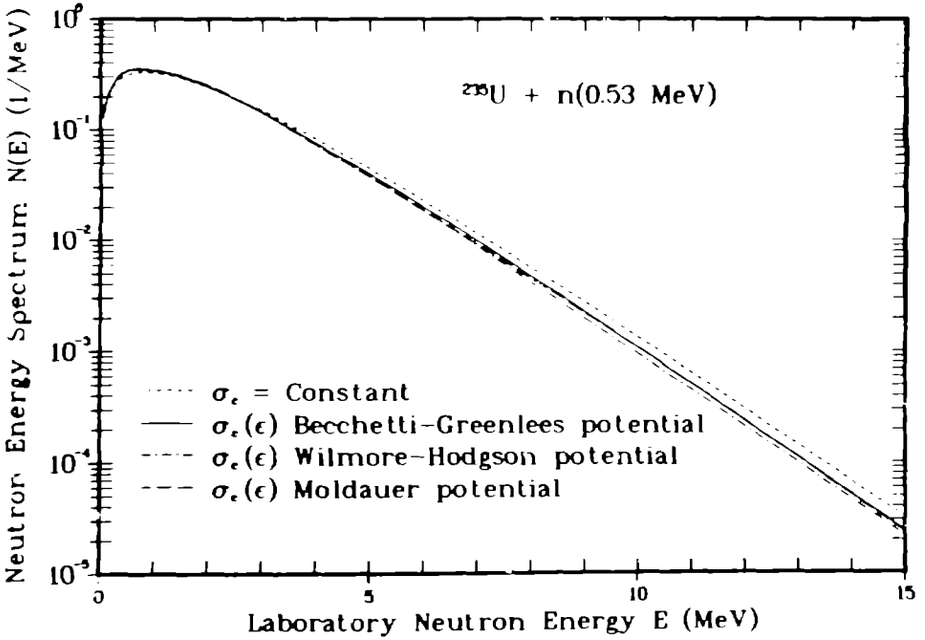
Neutron Energy Spectrum N(E) (1/MeV)
10^{0}
10^{-1}
10^{-2}
10^{-3}
10^{-4}
10^{-5}
^{235}U + n(0.53 MeV)
σ_ϵ = Constant
$\sigma_\epsilon(\epsilon)$ Becchetti-Greenlees potential
$\sigma_\epsilon(\epsilon)$ Wilmore-Hodgson potential
$\sigma_\epsilon(\epsilon)$ Moldauer potential
0
5
10
15
Laboratory Neutron Energy E (MeV)

Fig. 5.

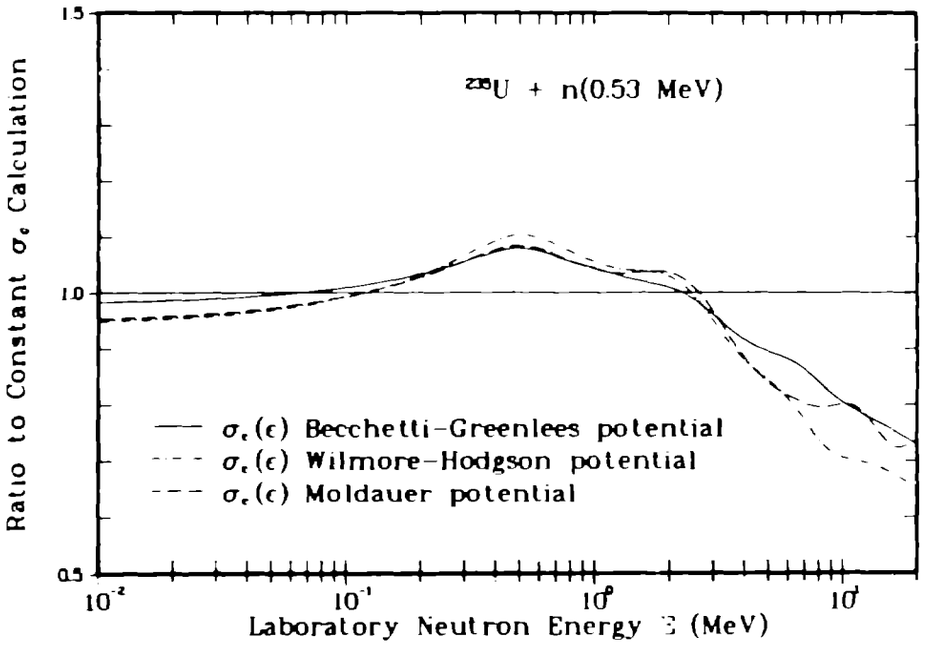
1.5
1.0
0.5
^{238}U + n(0.53 MeV)
Ratio to Constant σ_ϵ Calculation
$\sigma_\epsilon(\epsilon)$ Becchetti-Greenlees potential
$\sigma_\epsilon(\epsilon)$ Wilmore-Hodgson potential
$\sigma_\epsilon(\epsilon)$ Moldauer potential
10^{-2}
10^{-1}
10^{0}
10^{1}
Laboratory Neutron Energy E (MeV)

Fig. 6.

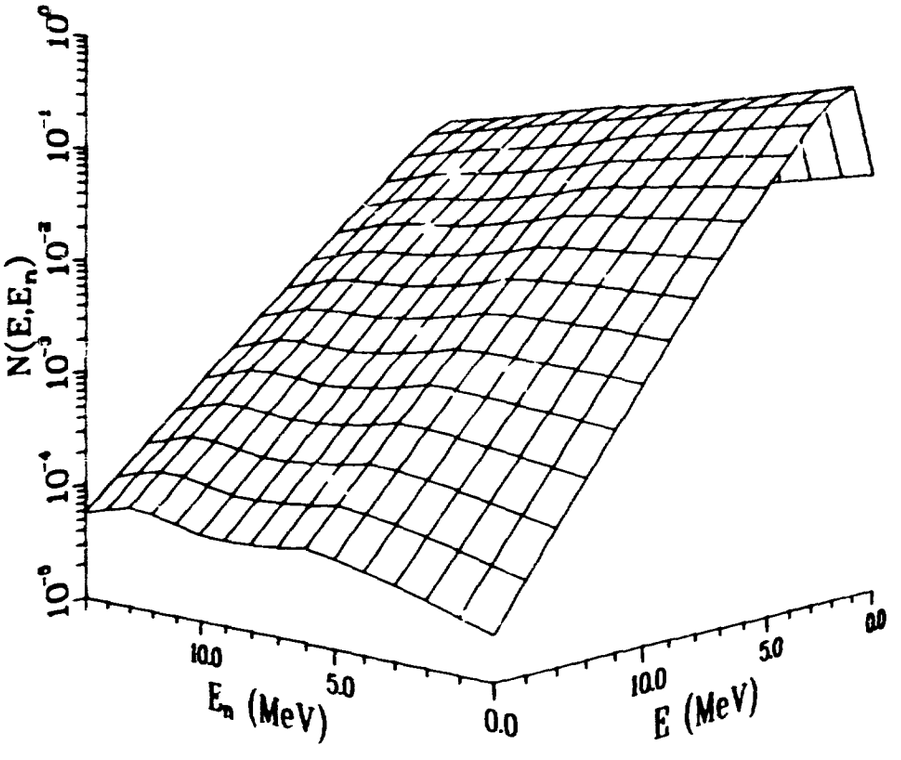

Fig. 7.

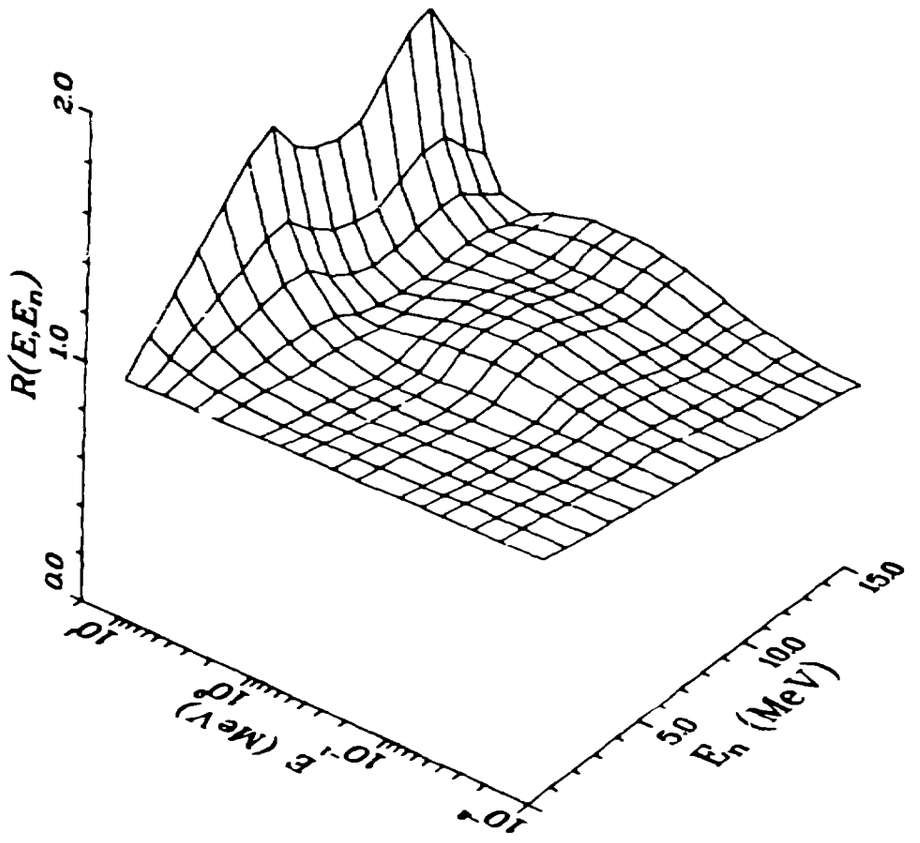

Fig. 8.

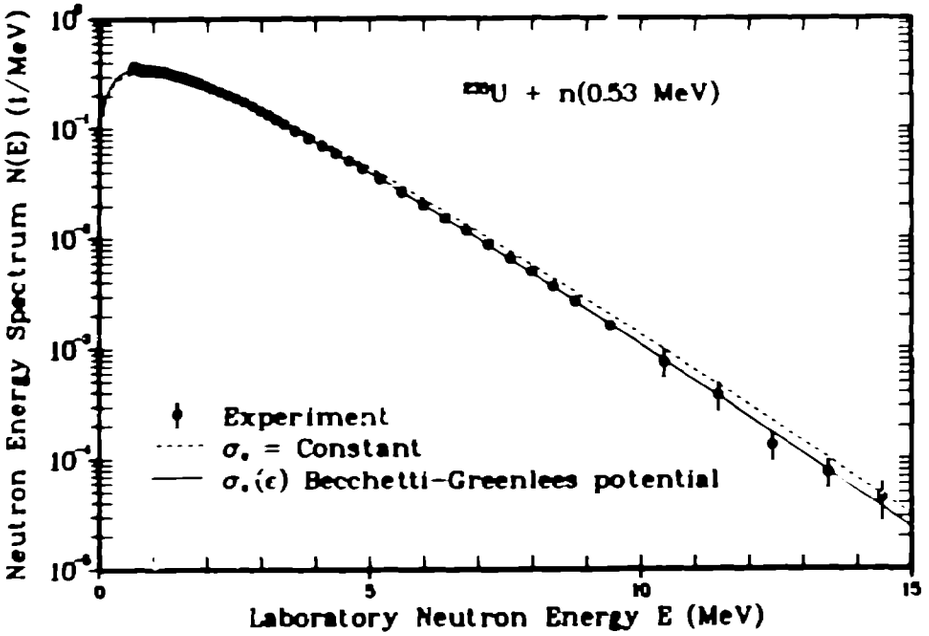
Neutron Energy Spectrum N(E) (1/MeV)
Laboratory Neutron Energy E (MeV)
^{235}U + n(0.53 MeV)
Experiment
σ_t = Constant
$\sigma_t(\epsilon)$ Becchetti-Greenlees potential
0
5
10
15

Fig. 9.

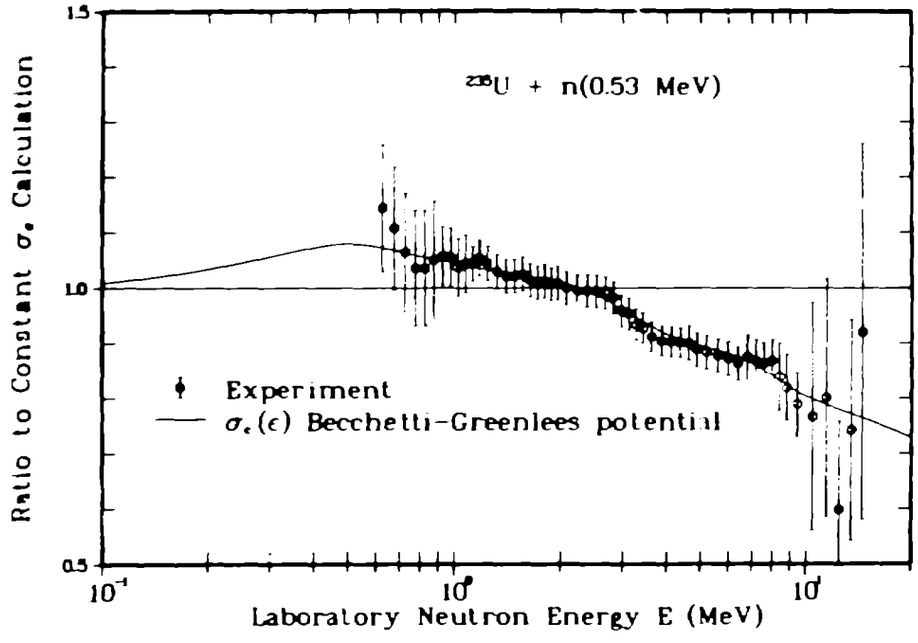
1.5
1.0
0.5
Ratio to Constant σ_e Calculation
^{238}U + n(0.53 MeV)
Experiment
$\sigma_e(\epsilon)$ Becchetti-Greenlees potential
10^{-1}
10^{0}
10^{1}
Laboratory Neutron Energy E (MeV)

Fig. 10.

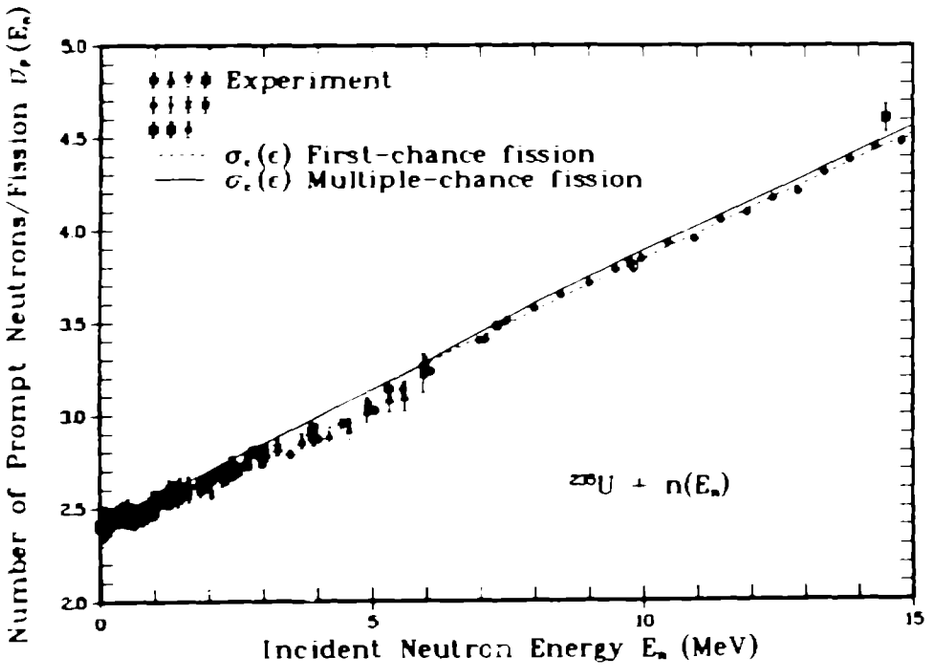
Experiment
$\sigma_c(\epsilon)$ First-chance fission
$\sigma_c(\epsilon)$ Multiple-chance fission
$^{235}U + n(E_n)$
Number of Prompt Neutrons/Fission $\bar{\nu}_p(E_n)$
Incident Neutron Energy E_n (MeV)
5.0
4.5
4.0
3.5
3.0
2.5
2.0
0
5
10
15

Fig. 11.

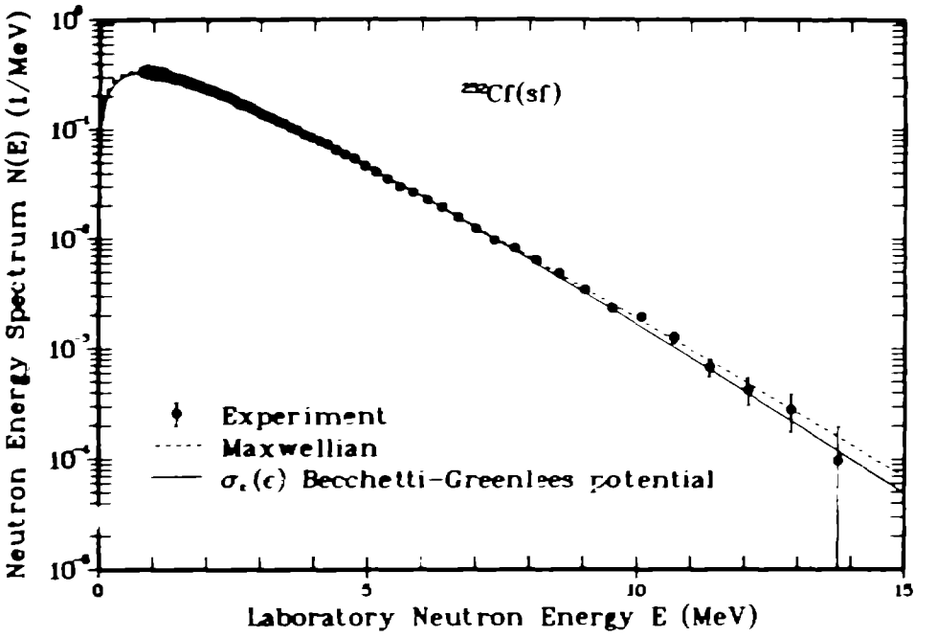
Neutron Energy Spectrum N(E) (1/MeV)
^{252}Cf(sf)
Experiment
Maxwellian
$\sigma_c(\epsilon)$ Becchetti-Greenlees potential
Laboratory Neutron Energy E (MeV)
0
5
10
15

Fig. 12.

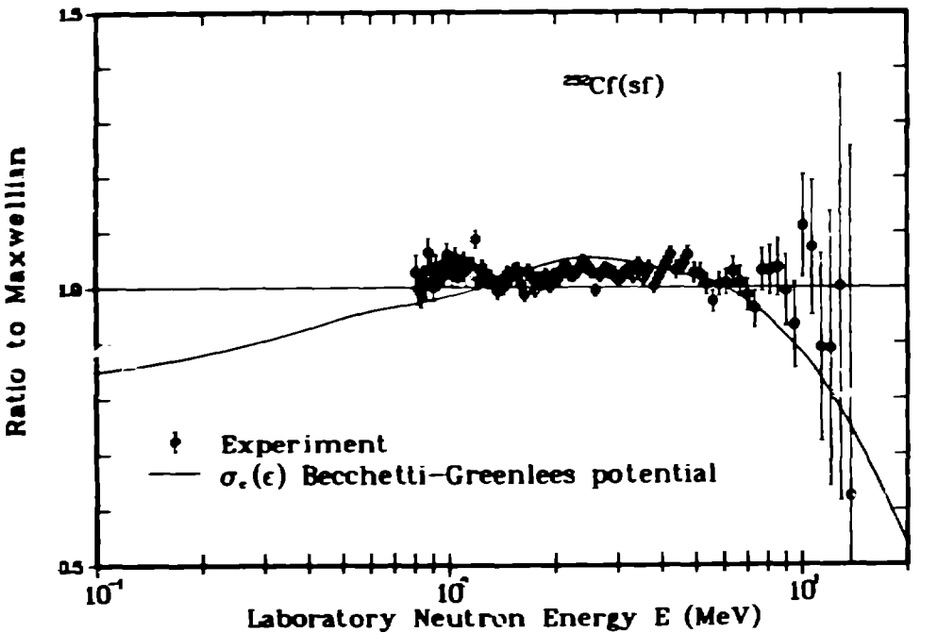
1.5
1.0
0.5
^{252}Cf(sf)
Ratio to Maxwellian
Experiment
$\sigma_c(\epsilon)$ Becchetti-Greenlees potential
10^{-1}
10^{0}
10^{1}
Laboratory Neutron Energy E (MeV)

Fig. 13.

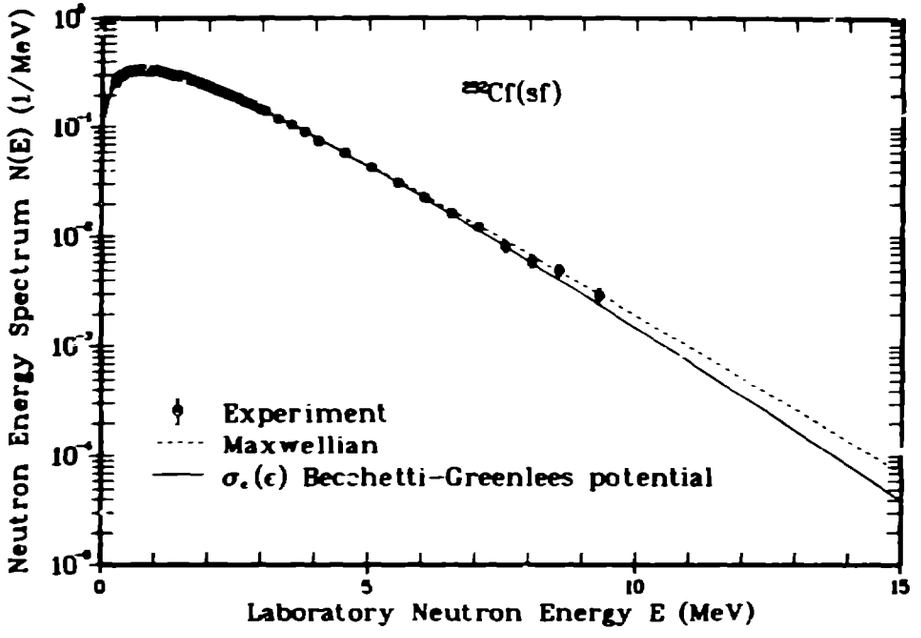
Neutron Energy Spectrum N(E) (1/MeV)
^{252}Cf(sf)
Experiment
Maxwellian
$\sigma_c(\epsilon)$ Becchetti–Greenlees potential
Laboratory Neutron Energy E (MeV)
0
5
10
15

Fig. 14.

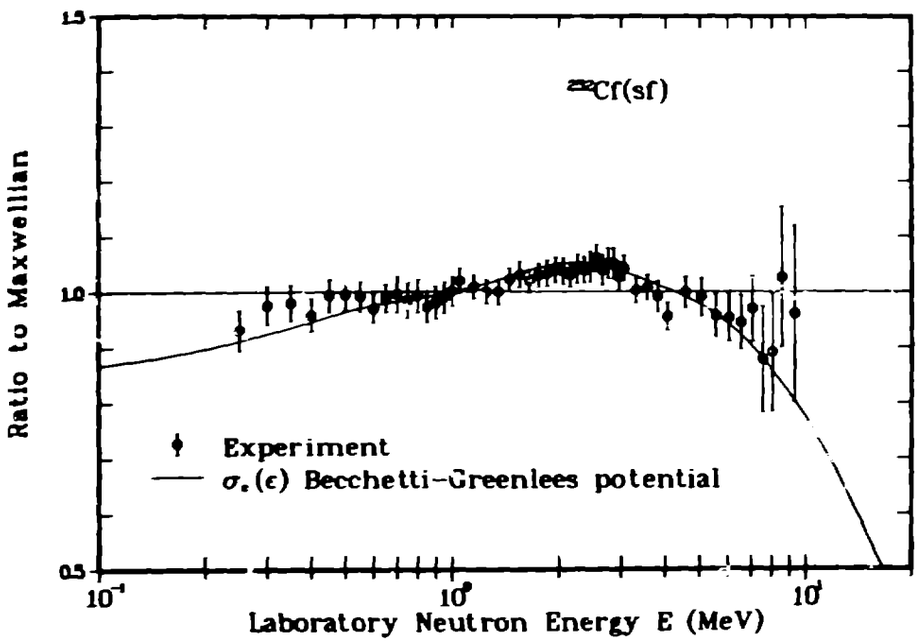
1.5
1.0
0.5
Ratio to Maxwellian
252Cf(sf)
Experiment
σ_e(ε) Becchetti-Greenlees potential
10^-1
10^0
10^1
Laboratory Neutron Energy E (MeV)

Fig. 15.